Thermal characterization of morphologically diverse copper phthalocyanine thin layers by scanning thermal microscopy

Dominika Trefon-Radziejewska, Justyna Juszczyk, Maciej Krzywiecki, Georges Hamaoui, Nicolas Horny, Jean-Stéphane Antoniow, Mihai Chirtoc

Ultramicroscopy 233 (2022) 113435

Contents lists available at ScienceDirect

Ultramicroscopy

journal homepage: www.elsevier.com/locate/ultramic

Thermal characterization of morphologically diverse copper phthalocyanine thin layers by scanning thermal microscopy

Dominika Trefon-Radziejewska [a,*], Justyna Juszczyk [a], Maciej Krzywiecki [a], Georges Hamaoui [c], Nicolas Horny [b], Jean-Stéphane Antoniow [b], Mihai Chirtoc [b]

[a] Institute of Physics Center for Science and Education, Silesian University of Technology, Konarskiego 22B, Gliwice 44-100, Poland
[b] ITheMM, Université de Reims Champagne-Ardenne URCA, Reims 51687 France
[c] ESYCOM UMR 9007, Université Gustave Eiffel, CNRS, CNAM, Marne-la-Vallée F-77454, France

ARTICLE INFO

Keywords:
Scanning thermal microscopy
Thermal probe
Thermophysical properties
Thermal imaging
Morphological properties
Copper phthalocyanine

ABSTRACT

Morphologically diverse copper phthalocyanine (CuPc) thin layers were thermally characterized by scanning thermal microscopy (SThM). The organic layers with thicknesses below 1 μm were deposited by physical vapor deposition in a high vacuum on the N-BK 7 glass substrates. Four set of samples were fabricated and studied. Atomic Force Microscopy imaging revealed strong differences in the surface roughness, mean grain size/height, as well as distances between grains for the CuPc layers. For quantitative thermal investigations, three active SThM operating modes were applied using either a Wollaston thermal probe (ThP) or KNT ThP as thermal probe heated with a DC, an AC (3ω-SThM) current or their combination (DC/AC SThM). Meanwhile, qualitative analysis was performed by thermal surface imaging. The results of this study revealed a correlation between the morphology and the local thermophysical properties of the examined CuPc thin layers. It was found that the heat transport properties in such layers will deteriorate with the increase of the surface roughness and porosity. Those results can be a valuable contribution to the further development of phthalocyanine-based devices.

1. Introduction

The usage of thin films and nanostructured materials in practical applications has been significantly increasing within the last two decades. New advances in heat management applications prompt the need to fully characterize these new components and find their electrical and thermophysical properties. Commonly, it has been known that the nanoscale heat transport affects the macroscopic thermal behavior of electronic devices. Smaller, faster, and more efficient electronic devices evince higher power consumption density and heat generation, increasing the risk of overheating the system. Hence, to properly design multiscale electronic devices, the knowledge of the materials' structure and thermophysical properties allow the thermal management of the systems preventing their thermal failure and extending their operation lifetime [1–3].

Furthermore, several studies show that the thermophysical properties of materials with thicknesses reaching down to the nanometers highly differ from their bulk analogues [1,4,5], which encourages the thermal re-examination at the nanoscale. At such small scales, the quality of the material's surface and interface begin to significantly affect the heat transport mechanisms. Consequently, a possible modification of the thermophysical properties of matter may appear according to an individual surface morphological variation [5,7,8]. This is of particular importance in the case of rough materials with developed surfaces and can become a real challenge in their thermal characterization. In literature, one can find several research on the correlation between morphology and local thermophysical properties of thin films. Morphology parameters affecting thermal properties are, among others, surface roughness, material porosity, grain arrangement in the layer, grain size, and boundaries between grains [7–12].

The studies cited above indicate clearly that the thermophysical properties of thin layers are related to their surface morphology and should be examined in accordance with their structure, especially for rough samples. Therefore, an appropriate method for local thermal and topography characterization with a nanometer range resolution is needed. Such high requirements are fulfilled by the means of scanning thermal microscopy (SThM), which is proven to be a key thermal characterization tool [13]. The SThM is an atomic force microscope

* Corresponding author.
E-mail address: Dominika.Trefon@polsl.pl (D. Trefon-Radziejewska).

https://doi.org/10.1016/j.ultramic.2021.113435
Received 3 February 2021; Received in revised form 28 September 2021; Accepted 25 November 2021
Available online 27 November 2021

(AFM) equipped with a thermal module and thermal probe (ThP) instead of a classical AFM tip. Among other types of thermal probes, thermoresistive probes are commonly used and commercially fabricated using several materials. The most common ones are the Wollaston ThP [14], the palladium [15] and the doped-silicon probes [16]. For thermophysical measurements, the heating of the sample by the probe operating in active mode (in DC or AC regimes) is required. The temperature sensor at the probe's tip apex is henceforth heated through Joule effect and plays the role of heat source for the sample. Hence, this technique allows the investigation of the thermal transport in nanoscale [17], thermal imaging [18,19] and determination of local thermophysical properties [20–22]. AFM surface topography imaging, performed with even higher spatial resolution (using a classical AFM probe), is used as a complementary method to SThM thermal measurements, enabling more insightful interpretation and analysis. Such combination between the thermal and morphology scans have already been applied in many works [6–12,23,24]. However, a significant part of them were performed for samples with quite smooth surfaces, for which the SThM thermal analysis is much simpler and accurate. One of the most substantial problems in microscopic thermal measurements for rough and porous materials is the analysis of heat transfer mechanism in the probe-sample system [21,25,26]. For active SThM mode working in ambient conditions (at room temperature and out of vacuum), the heat is transported from the probe heated region through three channels: (1) along the cantilever to the probe holder, (2) to the surroundings and (3) to the sample. The heat transfer from the probe to the sample is achieved via thermal radiation, water meniscus, thermal conduction through the surrounding gas, and direct solid-solid contact between the probe and the sample [21,25].

If the SThM system does not operate in vacuum, heat transfer via thermal radiation can be neglected [21]. It was also proven that, for the SThM Kelvin Nanotechnologies nanofabricated thermal probe (KNT ThP) used in this work, the water meniscus thermal conductance consists of about 6% of thermal contact conductance of probe–sample interaction [27]. While for Wollaston ThP, also used in this study, avoiding the water meniscus formation requires rising the operating temperature above 100 °C [28]. The contribution of the last mechanism in the total probe-sample heat flux depends on the thermal contact quality. In turn, the thermal contact quality depends on the sample surface [21,26]. Besides surface morphological effects, the contact area is also influenced by the size of the SThM probe apex radius. The above emphasized issues pose a challenge in determining the thermophysical properties of thin layers with a morphologically complex surfaces, as the spatial and temperature resolution of the SThM technique are limited in particular by the size of the tip, the sample properties and the tip-sample heat transfer mechanisms depending on the operation conditions [21,25] and sample's surface topography [29,30].

In this work, we focus on SThM thermal analysis of morphologically diverse thin copper phthalocyanine layers (CuPc). CuPc belong to a class of metal-centered phthalocyanine semiconductor organics applied in sensing and organic electronic devices due to its well-developed surface [31–34]. Their sensing properties are closely related to the active surface interacting with the given analyte [35], while their operating conditions depend on the thermal behavior in elevated temperatures. We are interested in a versatile analysis of SThM possibilities as a tool for local thermophysical properties determination in the case of rough organic layers. Our previous work was the first attempt to characterize the thermal properties of organic MePc layers with well-developed surfaces [10]. In this work, while investigating CuPc thin layers, we consider the spatial resolution of the SThM measurement by using two different types of probes operating in several measurement modes. We utilize three active SThM operation modes, utilizing different probe driving currents: DC (DC SThM), AC (3ω-SThM), and the combination of both (DC/AC SThM). The measurements are performed with two different resistive probes, varying in spatial resolution - the Wollaston ThP and the KNT ThP. Besides local thermal quantitative characterization, qualitative analysis is also performed by thermal surface imaging. The information about CuPc layers morphology is based on the AFM analysis. The goal of this study is an attempt of a comprehensive, qualitative, and quantitative thermal analysis of investigated CuPc rough, thin layers using three mentioned SThM operation modes along with the thermal and AFM imaging. Such a combined investigation will be relevant for future thermal management design and CuPc sensors development.

2. Materials and methods

2.1. Materials

The objective of the research is to study CuPc thin layers with deliberately designed different surface morphologies. The organic layers were deposited by physical vapor deposition in a high vacuum on the N-BK 7 glass substrates of thickness (830 ± 10) μm. Substrates were degreased with acetone in an ultrasonic bath, rinsed with deionized water and dried in a nitrogen stream prior deposition. The CuPc powders (Sigma-Aldrich, 99.7% dye content) were degassed before sublimation to remove residual contaminations and adsorbed water. The main samples numbered #1, #2 and #3 were obtained at the base pressure of deposition system $1.5{\cdot}10^{-7}$ Pa. The deposition rate was kept at the level of 1 Ås^{-1} as measured with a Prevac TMC 13 microbalance using standard 6 MHz gold plated quartz crystals. The differences in morphology for these three samples #1 (110 ± 20 nm), #2 (280 ± 20 nm) and #3 (400 ± 50 nm) were obtained by controlled, sequential deposition of successive CuPc layers on the substrates kept at 300 K. Sample #4 (900 ± 100 nm) was deposited during a single-stage process, with deposition rate 5–10 Å s^{-1}. Thicknesses of CuPc layers were verified by a profilometer (KLA Tencor, Alpha-Step IQ, USA).

2.2. Methods

2.2.1. AFM imaging

AFM surface imaging of the investigated samples was carried out using Park Systems PSIA XE-70 Microscope. The topography imaging was performed in a non-contact mode (NC-AFM) using a BS Tap300Al cantilever. For image processing Gwyddion 2.45 software [36] was used and surface topographical properties, such as root mean square of roughness (RMS), number of grains, mean grain size and total perimeter length were then analyzed [37,38].

2.2.2. SThM imaging

Thermal imaging was performed with the nanoscale thermoresistive metallic palladium probe KNT-SThM-2an (KNT ThP) alongside the thermal module of the Park Systems PSIA XE-70 microscope system. The active SThM mode (also called conductivity or conductance contrast mode) was chosen, as it is typically used for local thermal properties imaging. For these measurements, the probe, working in a Wheatstone bridge configuration, was heated with a DC current of 1.7 mA, which was kept constant during the scan. The SThM thermal signal, being a voltage drop along the probe, was then analyzed.

2.2.3. DC SThM

The DC SThM has been commonly used for thermal measurements and its detailed description can be found elsewhere [28]. In this experiment, ThP, driven by DC current, acts as a heater and a thermal sensor. As the heat flows from the probe to the sample, the probe temperature changes according to the sample's thermophysical properties. The DC SThM measurements were carried out using a Wollaston ThP in Wheatstone bridge configuration combined with an AFM system (2990 MicroTA, TA Instrument). The experiment was performed in a constant-temperature mode, where the probe temperature is maintained by the thermal module system, by altering the applied current during scanning. Heat flux from the probe to the surroundings, expressed by the

power dissipated on the probe, was determined. Probe signal in the air was measured as a reference, to reduce the influence of ambient temperature variations. The difference ΔP (mW) between the probe signals in contact with the sample surface P_c and in the air, P_a, was determined. The $\Delta P/ P_c$ was calculated and then analyzed. Signals from different surface areas were collected and averaged. Measurements were performed for probe temperatures 30 °C, 150 °C, and 200 °C.

2.2.4. 3ω-SThM

In the 3ω-SThM, the probe is heated by an AC current at a frequency ω. The corresponding Joule effect thermal phenomena occur at 2ω, resulting in a resistance alternation at 2ω. The 3ω component of probe voltage drop, being directly proportional to its AC temperature, is the measured signal. The most important advantage of this technique is the lock-in signal processing which enables higher sensitivity, stability, and resolution in comparison to the DC method. The method has been widely used for SThM measurements of local thermophysical properties [23,39,40]. The description of the method applied with the SThM Wollaston ThP can be found elsewhere [40]. The 3ω-SThM measurements were carried out by a resistive Wollaston ThP (Veeco Metrology Group, USA) working in a Wheatstone bridge configuration. The lock-in amplifier (Stanford Research Systems, SR865, USA) was used as a source of excitation signal as well as for measurement of the 3ω harmonic component of the probe voltage amplitude signal. The difference between signals registered for the probe brought in contact with the sample surface and in the air was analyzed.

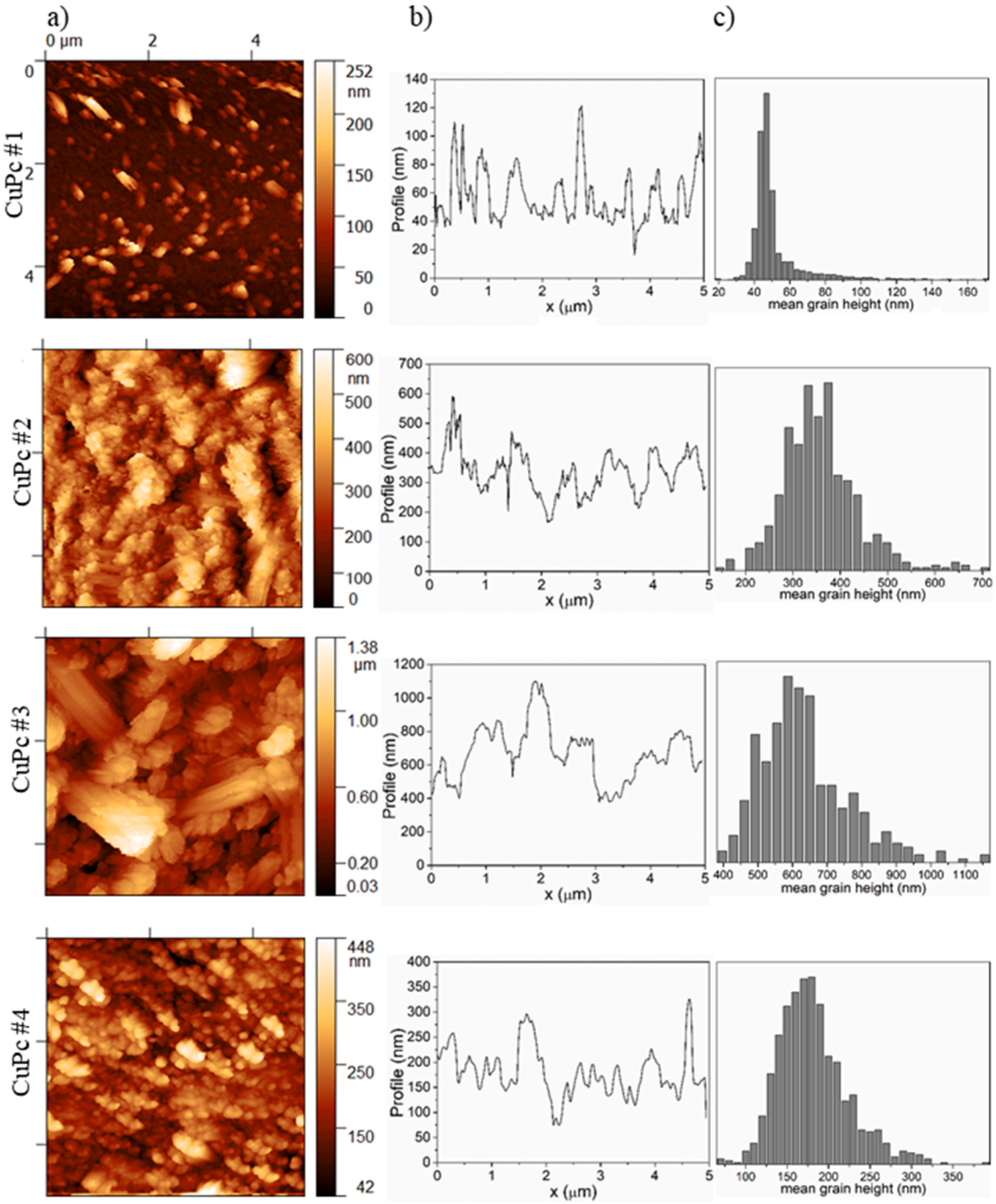

Fig. 1. (a) NC-AFM 5 × 5 μm^2 surface images, (b) profiles of the corresponding images, and (c) mean grain height histograms of CuPc samples. Measurements were performed by the KNT ThP.

2.2.5. DC/AC SThM

In the DC/AC SThM the probe works in active mode and the probe signal consists of two components. The probe is driven with a sum of DC current, and a small AC component superimposed to it. Such approach allows to combine the advantages of both measurement modes: well established and stable mechanical contact with the sample surface and maintaining the SThM signal sensitivity to the thermal properties of the investigated material. The DC/AC SThM was proposed by Bodzenta et al. [41] and successfully used for investigating thermal properties of SiO_2 [17,42] and ZnO [8] thin films, as well as W-Re and Mo-Re thin alloy layers [7]. In this operating mode, the determined values are probe static R_s and dynamic R_d resistances, registered in contact with the sample surface and out of contact, while the probe is in the air. It has been proven [41] that the ratio of these two resistances $(R_d-R_s)_{in}/(R_d-R_s)_{out}$ is correlated with the thermal properties of the sample. In this experiment the KNT ThP was used with the thermal module of the PSIA XE-70 microscope system.

3. Results

3.1. AFM imaging

The NC-AFM 5 × 5 μm^2 images of investigated CuPc layers together with their corresponding average profiles, and the mean grain height histograms are presented in Fig. 1. The sequential deposition of successive CuPc layers on the substrates contributed to relevantly diverse morphology among sample #1, #2, and #3 (Fig. 1a). Systematic accretion of grains and their significant expansion is observed as the thickness of subsequent CuPc layers increases. In the case of #3 CuPc sample, the notably elongated grains in the vertical direction begin to stack up generating air gaps between them. The histogram of grain height for sample #3 (Fig. 1c) approves the presence of expressively high and chaotically arranged grains, as well it shows a high heterogeneity of this layer. In turn, the AFM image, and the grain height histogram of #4 CuPc sample reveals the layer with rather evenly distributed grains. The profiles averaged from the AFM images (Fig. 1b) indicate, that as the size of the grains increases, the distance between them also increases. Hence, in order to analyze the surface morphological differences among the investigated CuPc layers, the quantitative parameters on the base of AFM imaging were determined and exposed in Table 1. While the root mean square of roughness (RMS), and the mean grain size parameters grow, the number of grains and the total perimeter length decrease, with increasing layer thickness for samples of #1, #2, and #3. Although the sample #4 exhibits the largest CuPc thickness, its surface roughness is intentionally right behind the thinnest sample #1, as a consequence continuous deposition process.

3.2. SThM imaging

SThM thermal images of investigated samples along with their corresponding probe thermal signal histograms are presented in Fig. 2. Well-developed surfaces, like the ones investigated, can pose some difficulties while maintaining thermal contact with the sample surface during scanning, especially for the thermal probe operating in the

Table 1
Surface topographical parameters determined for investigated CuPc layers.

CuPc	RMS (nm)	Number of grains	Mean grain size* (nm)	Total perimeter length** (nm)
#1	29	2015	55	466
#2	120	494	130	310
#3	207	433	134	297
#4	59	862	109	417

* Mean grain size denotes lateral crystallite size of CuPc samples.
** Total perimeter length is the perimeter indicating the overall length of the grain's outer boundary lines.

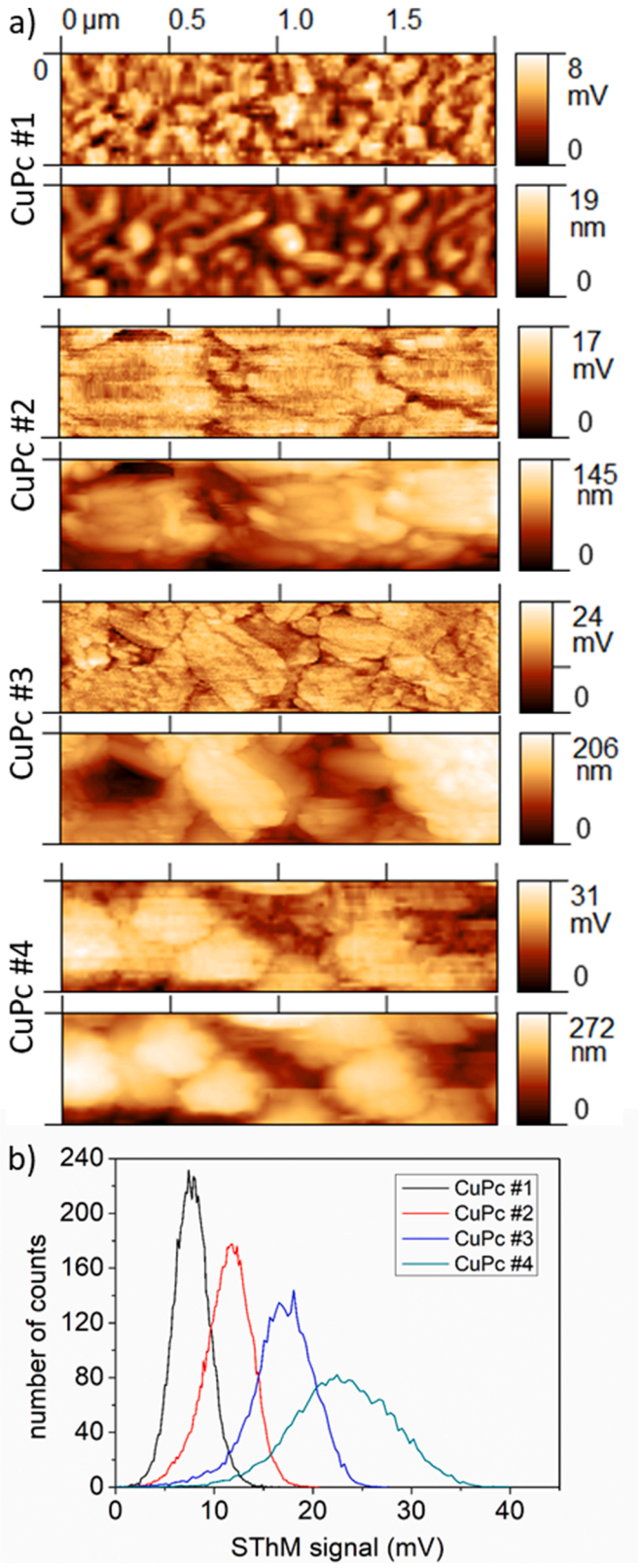

Fig. 2. (a) SThM thermal and topography images of investigated samples and (b) corresponding histograms of SThM signals. Presented thermal images are exemplary while the histograms are averaged over a larger number of similar images registered on the samples' surface. Thermal imaging was performed by the KNT ThP.

constant current mode. Therefore, obtaining images of large parts of the surface was not always possible for all our samples. However, obtained thermal images allow to visualize and analyze all the characteristic thermal properties of the tested surfaces. Before further analysis, all images were rescaled so that the minimum value of the SThM signal was equal to zero. Similarly, to the AFM images, sample #1 is characterized by the smallest and finest grains that tend to aggregate into larger agglomerates for samples #2 and #3. In the case of sample #1, the SThM histogram has the smallest scatter (dispersion) of the recorded thermal signal while at the same time the largest relative difference between the minimum and maximum recorded signal. In this case it can be concluded that there is a predominant value of the thermal signal and that it is relatively uniform for the entire surface. As the grain size and the RMS increase, for samples #2 and #3, respectively, it can be observed that the SThM histograms flatten, and the scatter of the recorded values of the thermal signal increases. In the case of sample #3, it was additionally observed that the histogram is not symmetrical. It has a greater share of values below the dominant. The largest signal dispersion and the smallest relative difference between thermal signals were observed for sample #4. Above observations result from many factors, from which one should definitely take into account the shape of the surface and how the thermal contact is arranged, what mechanisms will dominate it, the size of the characteristic surface features in relation to the size of the probe, etc. Recorded histograms can be helpful for predicting the uncertainty of quantitative measurements performed at random points on the surface. The greater the width of the histogram, the greater the uncertainty of the measurement is expected.

3.3. DC SThM

DC SThM measurements were performed for the set of CuPc samples #1, #2, and #3. The relative differences $\Delta P/ P_c$ for CuPc samples are illustrated in Fig. 3 and presented in Table 2.

The heat flux from the probe to the sample depends, among other factors, on the sample local thermal conductivity [28]. The higher the thermal conductivity of the sample, the more power is dissipated at the probe (and hence the greater the relative power ratio) in order to ensure a constant probe temperature.

3.4. 3ω-SThM

3ω-SThM measurements were performed for all the CuPc samples at ambient temperature. As it was mentioned in paragraph 2.2.4, the 3ω harmonic component of the Wollaston ThP voltage amplitude signal U was measured for CuPc and for reference samples in contact with their surface and in the air. In order to estimate the thermal conductivity, κ, of the CuPc samples these signals were subtracted, and a calibration curve was generated for reference materials of known thermal conductivity values (Fig. 4 and Table 3).

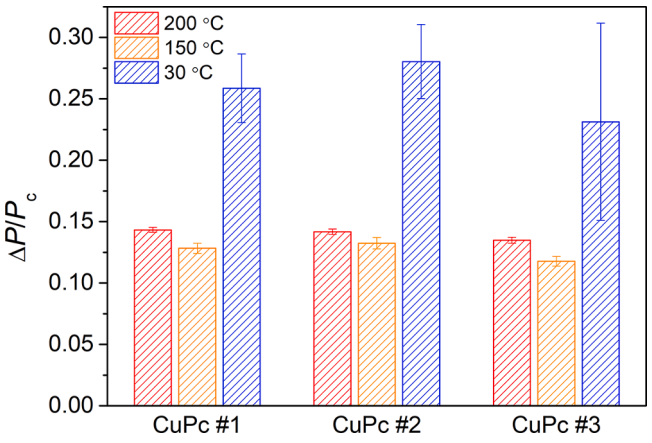

Fig. 3. DC SThM experimental results measured for CuPc samples at different Wollaston probe temperatures. Measurements were performed by the Wollaston ThP.

Table 2
The experimental values of $\Delta P/P_c$ determined for CuPc samples at different Wollaston ThP temperatures.

CuPc	Probe temperature 200 °C $\Delta P/P_c$	150 °C $\Delta P/P_c$	30 °C $\Delta P/P_c$
#1	0.1432 ± 0.0020	0.1283 ± 0.0041	0.2586 ± 0.0280
#2	0.1418 ± 0.0022	0.1324 ± 0.0047	0.2803 ± 0.0301
#3	0.1348 ± 0.0025	0.1177 ± 0.0040	0.2312 ± 0.0803

It should be noted, that the κ obtained for CuPc samples directly from the calibration curve are the apparent thermal conductivities (κ_a) due to the influence of the substrate thermal properties on the SThM thermal signal (Table 3, column 3). To remove the substrate influence, the κ_a values were subjected to the SThM correction procedure basing on the thermal spreading resistance analysis [42]. Such procedure is particularly important in the case of thin layers, which thicknesses are comparable to or smaller than the probe-sample contact diameter. In the system consisting of a single layer on a substrate, the κ_a value of the layer can be corrected through numerical calculations taking into consideration the thickness of the layer, the κ of the substrate and the size of the probe-sample thermal contact radius. All details concerning the correction procedure can be found in Ref. [42]. The following parameters were necessary for the correction: κ_a, CuPc layer thickness, κ of the substrate (1.1 W m^{-1}K^{-1}), and the contact radius of the Wollaston ThP. Due to the fact, that the radius of the Wollaston ThP is estimated to be between 800 nm and over 1 μm [43], three values were considered in the calculations: 800 nm, 900 nm, and 1000 nm. The corrected thermal conductivities (κ_c) for CuPc layers are listed in Table 3, column 4, and presented in Fig. 5. The possible error in estimating the probe radius within the order of 10%, with respect to the central value of 900 nm, will not cause the κ_c value to exceed the range adopted according to the uncertainty of the SThM measurement. The greatest impact on the κ_c value has the accurate estimation of the κ_a and its uncertainty. Since the calibration curve constructed on the basis of measurements taken by the Wollaston ThP becomes less sensitive above 1 W m^{-1}K^{-1}, the κ_c

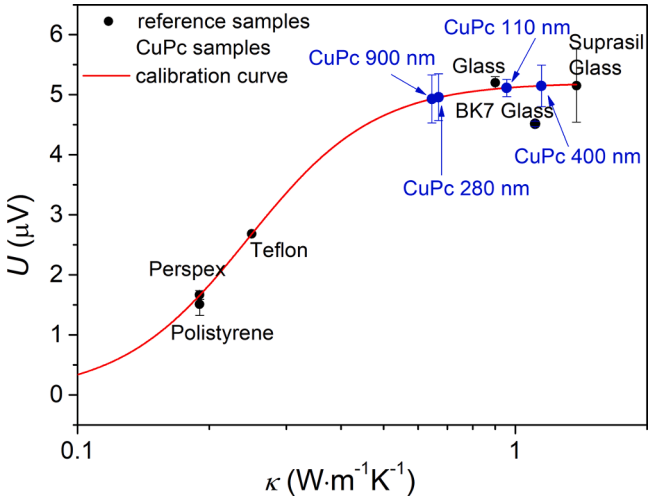

Fig. 4. 3ω-SThM experimental results measured for CuPc samples (blue dotes) and reference materials (black dotes) at ambient temperature. Measurements were performed by the Wollaston ThP. (For interpretation of the references to color in this figure legend, the reader is referred to the web version of this article.)

Table 3
The values of 3ω-SThM signal measured for CuPc samples and reference materials at ambient temperature (column 2). Estimated values κ_a on the base of 3ω-SThM calibration curve (column 3) and their corrected values κ_c determined from correction procedure (column 4). Below reference materials used for creating the calibration curve and their κ values.

CuPc	U (μV)	κ_a (W•m^{-1}K^{-1})	κ_c
#1	5.11 ± 0.14	0.96 ± 0.27	0.52
#2	4.96 ± 0.39	0.67 ± 0.19	0.23
#3	5.15 ± 0.35	1.15 ± 0.59	1.25
#4	4.93 ± 0.40	0.64 ± 0.18	0.32

Reference sample	U (μV)	κ (W•m^{-1}K^{-1})
Substrate BK7	4.515 ± 0.045	1.11
Glass	5.2 ± 0.10	0.90
Suprasil glass	5.15 ± 0.61	1.38
Teflon	2.685 ± 0.010	0.25
Perspex	1.51 ± 0.19	0.19
Polistyrene	1.665 ± 0.075	0.19

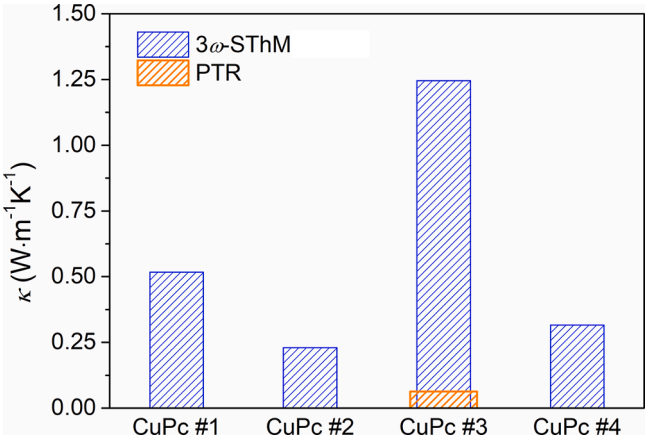

Fig. 5. The values of κ_c obtained from correction procedure implemented for 3ω-SThM measurements for CuPc samples. Measurements were performed by the Wollaston ThP. The κ_c value of CuPc #3 extracted from PTR is also reported for comparison.

determination for sample #2 and #3 results in uncertainties reaching up 59% and 86%, respectively, while for CuPc #1 is only 25%. In the case of CuPc sample #3, we had the opportunity to compare the obtained κ_c value to measurements made by using photothermal radiometry (PTR). The detailed description of the PTR method [44,45] and of κ extracting from the PTR signal can be found in Ref. [10]. The κ obtained from this method for CuPc #3 sample turned out to be equal to 0.063 W m^{-1}K^{-1} (placed in the Fig. 5). Such low κ value occurs for solid phase materials with an intrinsic κ lower than 1 W m^{-1}K^{-1} combined with a significant pore volume fraction [46]. Despite the sample #3 revealed the most rough and porous structure among the other ones, this result still seems to be too low. However, the PTR result reflects the trend observed in DC SThM, and in the next AC/DC SThM measurements, which allows us to conclude, that value of κ_c for CuPc #3 from 3ω-SThM is doubtful.

3.5. DC/AC SThM

The DC/AC SThM measurements were carried out for all the CuPc samples. The probe signal DC component was 1.7 mA, while the AC component was 0.085 mA. For the measurements taken out of contact the probe was lifted 2.0 mm in the air above the sample surface. In-contact measurements were taken at different surface areas and then averaged. The DC/AC SThM investigations were carried out at ambient temperature. Obtained results are illustrated in Fig. 6 and shown in Table 4. The difference between dynamic and static electrical resistances of the KNT ThP in the low frequency limit is proportional to the probe-sample thermal contact resistance, which at stable ambient conditions depends only on the thermal resistivity R_{th} of the sample [41]. Hence, higher values of DC/AC SThM signal correspond to higher values of sample's R_{th}, and lower sample thermal conductivity.

4. Discussion

The SThM investigations carried out on morphologically diverse CuPc thin layers revealed differences in their local thermophysical properties. The application of different SThM working modes like DC SThM, 3ω-SThM, and DC/AC SThM, but also ThPs with different spatial resolution allowed a broader and more insightful view of this problem. In Fig. 7 the thermal results obtained from all SThM methods at ambient temperature were correlated with RMS parameter of individual CuPc layer. The following regularity emerges from the above SThM studies. Local thermophysical properties deteriorate with increasing roughness of the CuPc layers. Therefore, the results in Fig. 7 were intentionally ranked in terms of increasing roughness, not layer thickness. The thermophysical properties of CuPc layers should not depend yet on the layer thickness in this thickness range. Jin et al. did not observe such thermal conductivity thickness dependence in CuPcs down to 10 nm [47,48]. It confirms that the differences in thermal results of investigated CuPc samples obtained by the means of methods used in this work follow from their diverse morphology, and not from the thickness.

One should realize, that in our studies only 3ω-SThM method allowed us to determine the specific κ of CuPc layers without the influence of the thermal signal deriving from the substrate itself. The obtained results clearly revealed deterioration of κ with increasing RMS of CuPc layers. The κ value of sample #3 in the Fig. 7 comes, however, from PTR measurement, because its value received from 3ω-SThM method was highly uncertain. This can be an effect of too deep penetration of the probe through the layer into the substrate. In the case of using the Wollaston ThP for soft organic samples, such a risk is probable. Another possible reason, suggested by AFM imaging, can be the presence of cavities in sample #3 filled with mixture of air and water inflating the SThM signal. In the case of DC/AC SThM the information about thermal resistivities (R_{th}) of CuPc layers was obtained. However, due to its inverse proportionality to the κ, one can observe gradual decreasing of thermal conductivity in CuPc samples with increasing RMS (Fig. 7). Although in DC/AC SThM measurements the thermal signal from the substrate couldn't be separated from the one coming from CuPc layer, the thermal results should not be significantly affected, as the KNT ThP

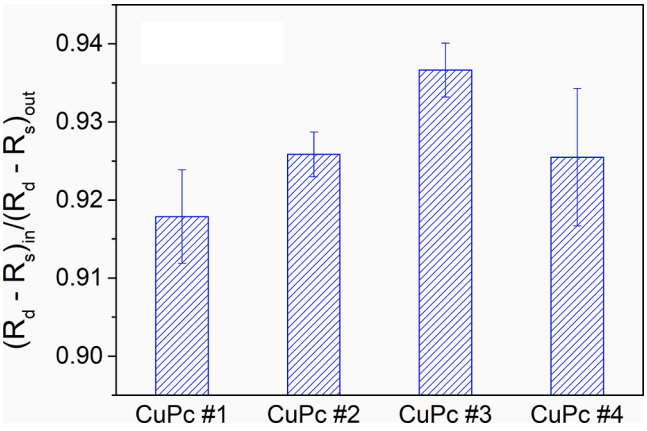

Fig. 6. AC/DC SThM experimental results measured for CuPc samples at ambient temperature. Measurements were performed by the KNT ThP.

Table 4
The values of DC/AC SThM signal determined for CuPc samples at ambient temperature.

CuPc	$(R_d-R_s)_{in}/(R_d-R_s)_{out}$
#1	0.9179 ± 0.0060
#2	0.9258 ± 0.0029
#3	0.9366 ± 0.0034
#4	0.9255 ± 0.0088

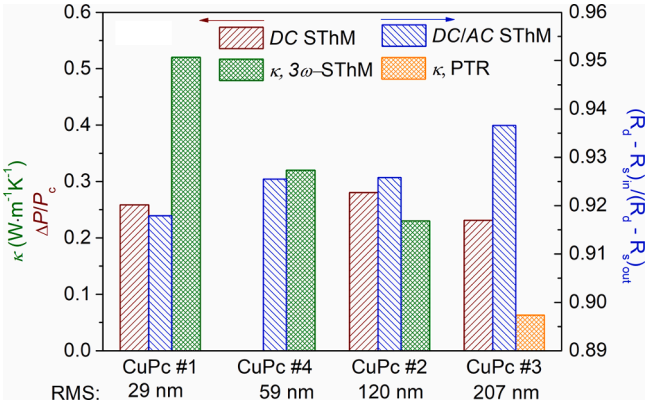

Fig. 7. Local thermal properties obtained from SThM measurements at ambient temperature for CuPc thin layers correlated with their RMS parameter.

thermal contact radius is about a hundred times smaller than Wollaston ThP. The elimination of substrate's part in the total thermal signal was also impossible in the case of DC SThM studies performed for the group of #1 – #3 samples. The obtained relative ratio of the power dissipated at the Wollaston ThP refers to the whole sample and is to a certain extent overestimated (Fig. 7). The smallest power ratio ($\Delta P/P_c$), i.e., the lowest thermal conduction, was determined for sample #3 with the highest RMS, which is in line with the observations from the other methods.

Diminishing local thermophysical properties with increasing RMS can wonder, especially when finding studies in the literature [8,9] dealing with correlation between thermal and morphology properties and showing an opposite tendency. However, it should be noted, that in work [8] the RMS was changing barely from 1.11 to 2.62 nm for ZnO films, and from 2.4 to 8.7 nm for FePc in work [9]. The values of RMS for our CuPc layers (Table 2) are in the range from 29 to 207 nm, which shows a significant variation of morphology and possible involvement of different thermal transport mechanisms. Despite increasing of the mean grain size and thus reducing the total perimeter length parameter, indicating the overall length of the grain's outer boundary lines, the heat transport deteriorates instead of improving in the case of samples #1–#3. The most resonable explanation of such behavior can be in the simultaneous grow of the porosity along with RMS increase. Sequential deposition of increasingly thicker CuPc layers one after the another caused vertical grain accumulation, which can be observed in AFM images in the Fig. 1a, as well as in the mean grain height histograms in Fig. 1c. As a result the elongated grains begin to lay down on each other creating stacks with lots of air gaps between them in sample #3 (Fig. 1a).

Worth noticing is, that the maxima of mean grain height histograms for all CuPc samples are well corellated with their thermal properties. With larger and higher grains, the surface porosity of CuPc layers increases, which can be seen in the profiles obtained from corresponding AFM topology images (Fig. 1b). Based on profiles, the free space between grains gradualy grows as RMS increases. This can be the main reason of thermal properties degradation in our case. The sample #4, although obtained in a separate deposition process, fits with all its morphological parameters in the above-mentioned relationships and ranks between sample # 1 and # 2. The similar impact of growing porosity and roughness on local thermal properties was observed for metal phthalocyanine layers in our previous work [10]. These two morphology parameters influence especially SThM results, because they change probe-sample heat transfer through altering the share of particular heat transfer mechanisms in the total probe-sample heat flux. Among four mechanisms of the total probe-sample heat flux mentioned in the introduction, the direct solid-solid contact depends on thermal contact quality, thus on sample surface quality. Previous researchers tried to quantify the effect of the sample's surface roughness on the thermal conductivity/conductance measurement. The answer is not trivial, however, the problem is linked to two effects: (1) the impact of the surface roughness on the samples' thermal properties and (2) the impact of the roughness on the probe-sample heat flow. These effects cannot be clearly separated [25]. Some analytical modeling based on the analysis of the thermal balance of the "probe-sample-environment" system while the probe is either out of contact or in contact with the sample were developed [25,49,50]. For the first effect it was found that the thermal contact and subsequently its thermal resistance strongly depend on parameters of the sample surface such as roughness [25,51]. Nonetheless, this effect is not fully quantified yet, and is currently a hot ongoing topic [52]. For the second effect, the impact of the roughness on the heat flow between probe and sample, can be limited to the heat flux through solid-solid contact. Recent study [53] showed that for Wollaston ThP and KNT ThP, the heat flux shared between the probe and the sample in the close vicinity of the sample surface (solid-solid, water meniscus, radiative transfer and short-range ballistic conductance through air) is around 19% and 11% (± 5%) and the heat flux going through air to the sample is around 13% and 21% (± 5%), respectively for each probe. All the remaining heat flux is just lost via air conduction or through the probe's cantilever. As the sensitivity of the SThM on sample thermal properties is already narrowed to such a small fraction of useful heat flux, its further reduction due to the roughness effect will be manifested in the measured signal, possibly amplifying the measurement uncertainties.

In porous and rough samples, the effective direct contact area with the SThM probe decreases, and the contribution of heat conduction through the surrounding gas starts to prevail over solid-solid heat conduction, diminishing the effectiveness of the probe-sample heat transport and affecting thermal results. Furthermore, one can observe, that the effective contact area depends on the ratio of the probe resolution to the distances between grains. When the size of the probe diameter is comparable or higher than the distances between grains, the changes in the SThM signal are more pronounced and so are the differences in obtained thermal properties regarding morphology variation. In that case, larger probe diameter allows to obtain more representative SThM signal coming from the area reflecting the real morphology with grains separated by air gaps. Relative drops in $\Delta P/P_c$ measured by the Wollaston ThP in DC SThM at ambient temperature reaches 8% and 11% for #2 and #3 CuPc samples in comparison to #1, while for KNT ThP with its resolution about one hundred higher, the changes in thermal signal are slighter. Because the KNT ThP diameter is comparable to the mean grain size (Table 1), and much smaller than distances between grains in CuPc layers, more often it has direct contact with the entire grain than with the air gaps between grains. The SThM signal registered by the KNT ThP seems to contain a different ratio of solid-solid heat conduction to conduction through surrounding air gaps than in the case of Wollaston ThP. Thus, the relative changes of CuPc thermal properties obtained by the KNT ThP may vary. However, they reflect the common trend.

Thermal signal histograms received from SThM imaging performed by the KNT ThP show thermal homogeneity of investigated CuPc layers and they explain the uncertainties of thermal properties measured by the DC/AC SThM. The worst thermal homogeneity is observed for sample #4 regarding its thermal histogram. This corresponds well with the size of measured R_{th} uncertainty for that sample (Fig. 6 and Table 4).

Significant uncertainties occur as well for all CuPc samples from the set #1–#3 in DC SThM method performed with the Wollaston ThP at

ambient temperature, especially when compared to analogous measurements at higher ones (Fig. 3 and Table 2). This can be related with the presence of water meniscus and its influence on probe-sample heat transfer at temperatures lower than 100 °C. It is well seen in the Fig. 3, that DC SThM results obtained at 150 °C and 200 °C are much more stable, consistent, and repeatable. They seem to be less dependent on morphology differences between CuPc samples, although they still confirm the decreasing trend for their thermal properties. When the thermal stability of investigated material allows, it is preferable to perform the SThM measurements with the use of Wollaston ThP at temperature high enough to avoid the water meniscus. In turn, the SThM signal registered by the KNT ThP is affected by the conductance of water meniscus to a minor extent even at room temperature [27].

5. Conclusions

Within this study we measured experimentally the thermophysical parameters (like $\Delta P/ P_c$, κ, and R_{th}) via SThM and we established their correlation to the studied material's morphology. The results obtained using the SThM technique, through several operating modes and with two types of thermal probes, showed the deterioration of the local thermal properties with the increase of both the surface roughness and the distances between grains. However, this dependency is better reflected in SThM measurements performed with Wollaston ThP than for KNT ThP. This result can be related with the ratio of their spatial resolutions to the mean grain size and the distance between grains in individual CuPc layers. The Wollaston ThP, due to its size, captures more collective, averaged thermal signal, reflecting characteristic morphological features of investigated CuPc layers. In turn, in the SThM studies using the KNT ThP, with its tip size comparable to the mean grain size and smaller than the distances between grains, the collected thermal signal is more local. As a result, the changes in morphology do not affect obtained thermal results in the same extent as in the case of studies performed with the Wollaston ThP. The stability of SThM signal collected by the KNT ThP is higher and water meniscus conduction independent. The stability of the SThM measurements can be improved at temperatures above 100 °C as long as the examined material is thermally stable at high temperatures.

Summarizing, the SThM studies for rough and porous samples offer a lot of possibilities for their local thermal characterization, however the selection of the appropriate measurement method and analysis are not trivial and require further development.

Declaration of Competing Interest

The authors declare the following financial interests/personal relationships which may be considered as potential competing interests.

Acknowledgments

The authors thank the Silesian University of Technology for the grant 14/030/BKM20/0007. The work was supported through the PHC Polonium 2015/2016 (project number 33564VE). MK acknowledges Institute of Physics – CSE statutory funds (14/030/BK-20/0005). The authors acknowledge ESPEFUM laboratory (at Institute of Physics – CSE, Silesian University of Technology) for access to SThM and AFM experimental setup, as well UMR FARE (INRA Reims University) for making their SThM experimental setups available.

References

[1] D.G. Cahill, W.K. Ford, K.E. Goodson, G.D. Mahan, A. Majumdar, H.J. Maris, R. Merlin, S.R. Phillpot, Nanoscale thermal transport, J. Appl. Phys. 93 (2003) 793–818.
[2] J. Bodzenta, Nanoscale heat transport, Mater. Sci. Pol. 26 (2008) 95–103.
[3] P. Tovee, M. Pumarol, D. Zeze, K. Kjoller, O. Kolosov, Nanoscale spatial resolution probes for scanning thermal microscopy of solid state materials, J. Appl. Phys. 112 (2012), 114317.
[4] S.R. Choi, D. Kim, S.H. Choa, S.H. Lee, J.K. Kim, Thermal conductivity of AlN and SiC thin films, Int. J. Thermophys. 72 (2006) 896–905.
[5] D. Cahill, P. Braun, C. Chen, D. Clarke, S. Fan, K. Goodson, P. Keblinski, W. King, G. Mahan, A. Majumdar, H. Maris, S. Phillpot, E. Pop, L. Shi, Nanoscale thermal transport. II. 2003–2012, Appl. Phys. Rev. 1 (2014), 011305.
[6] K. Fladischer, V. Leitgeb, L. Mitterhuber, G.A. Maier, J. Keckes, M. Sagmeister, S. Carniello, S. Defregger, Combined thermo-physical investigation of thin layers with Time Domain Thermoreflectance and scanning thermal microscopy on the example of 500nm thin, CVD grown tungsten, Thermochim. Acta 681 (2019), 178373.
[7] D. Trefon-Radziejewska, J. Juszczyk, A. Fleming, J. Podwórny, M. Chirtoc, N. Horny, A. Wrona, M. Lis, M. Mazur, D. Wojcieszak, D. Kaczmarek, J. Bodzenta, Thermophysical properties of refractory W-50.4%Re and Mo-39.5%Re thin alloy layers deposited on silicon and silica substrates, Int. J. Refract. Met. Hard Mater. 87 (2020), 105147.
[8] A. Kaźmierczak-Bałata, J. Bodzenta, M. Guziewicz, Microscopic investigations of morphology and thermal properties of ZnO thin films grown by atomic layer deposition method, Ultramicroscopy 210 (2020), 112923.
[9] M. Krzywiecki, L. Grządziel, J. Juszczyk, A. Kaźmierczak-Bałata, A. Erbe, J. Bodzenta, Correlation between morphology and local thermal properties of iron (II) phthalocyanine thin layers, J. Phys. D Appl. Phys. 47 (2014), 335304.
[10] D. Trefon-Radziejewska, J. Juszczyk, A. Fleming, N. Horny, J.S. Antoniow, M. Chirtoc, A. Kaźmierczak-Bałata, J. Bodzenta, Thermal characterization of metal phthalocyanine layers using photothermal radiometry and scanning thermal microscopy methods, Synth. Met. 232 (2017) 72–78.
[11] P. Veluswamy, S. Sathiyamoorthy, K.H. Chowdary, O. Muthusamy, K. Krishnamoorthy, T. Takeuchi, H. Ikeda, Morphology dependent thermal conductivity of ZnO nanostructures prepared via a green approach, J. Alloy. Compd. 695 (2017) 888–894.
[12] S. Gomès, L. David, V. Lysenko, A. Descamps, T. Nychyporuk, M. Raynaud, Application of scanning thermal microscopy for thermal conductivity measurements on meso-porous silicon thin films, J. Phys. D Appl. Phys. 40 (2007) 6677–6683.
[13] J. Bodzenta, Scanning thermal microscopy – a tool for thermal measurement in the nanoscale, Front. Nanosci. 14 (2019) 181–213.
[14] R.J. Pylkki, P.J. Moyer, P.E. West, Scanning near-field optical microscopy and scanning thermal microscopy, Jpn. J. Appl. Phys. 33 (6S) (1994) 3785.
[15] P.S. Dobson, J.M. Weaver, G. Mills, New methods for calibrated scanning thermal microscopy (SThM), in: Proceedings of the IEEE Sensors, 2007, pp. 708–711.
[16] B. Nelson, W. King, Measuring material softening with nanoscale spatial resolution using heated silicon probes, Rev. Sci. Instrum. 78 (2) (2007), 023702.
[17] J. Bodzenta, J. Juszczyk, A. Kaźmierczak-Bałata, P. Firek, A. Fleming, M. Chirtoc, Quantitative thermal microscopy measurement with thermal probe driven by DC+AC current, Int. J. Thermophys. 37 (2016) 73.
[18] F. Menges, P. Mensch, H. Schmid, H. Riel, A. Stemmer, B. Gotsmann, Temperature mapping of operating nanoscale devices by scanning probe thermometry, Nat. Commun. 7 (2016) 10874.
[19] L.C. Wei, J.A. Malen, Hot-spot thermal management by phase change materials enhanced by spatially graded metal meshes, Int. J. Heat Mass Trans. 150 (2020), 119153.
[20] K. Fladischer, V. Leitgeb, L. Mitterhuber, G.A. Maier, J. Keckes, M. Sagmeister, S. Carniello, S. Defregger, Combined thermo-physical investigations of thin layers with time domain thermoreflectance and scanning thermal microscopy on the example of 500 Nm thin, CVD grown tungsten, Thermochim. Acta 681 (2019), 178373.
[21] Y. Zhang, W. Zhu, F. Hui, M. Lanza, T. Borca-Tasciuc, M.M. Rojo, A review on principles and applications of scanning thermal microscopy (SThM), Adv. Funct. Mater. 30 (2020), 1900892.
[22] J. Bodzenta, A. Kaźmierczak-Bałata, K. Harris, Quantitative thermal measurement by the use of scanning thermal microscope and resistive thermal probes, J. Appl. Phys. 127 (2020), 031103.
[23] D. Trefon-Radziejewska, G. Hamaoui, M. Chirtoc, N. Horny, V. Smokal, A. Biitseva, O. Krupka, Beata derkowska-zielinska, thermophysical properties of methacrylic polymer films with guest-host and side-chain azobenzene, Mater. Chem. Phys. 223 (2019) 700–707.
[24] A. Kaźmierczak-Bałata, J. Bodzenta, M. Krzywiecki, J. Juszczyk, J. Szmidt, P. Firek, Application of scanning microscopy to study correlation between thermal properties and morphology of $BaTiO_3$ thin films, Thin Solid Films 545 (2013) 217–221.
[25] S. Gomès, A. Assy, P.O. Chapuis, Scanning thermal microscopy: a review, Phys. Status Solidi A 212 (2015) 477–494.
[26] C. Metzke, W. Frammelsberger, J. Weber, F. Kühnel, K. Zhu, M. Lanza, G. Benstetter, On the limits of scanning thermal microscopy of ultrathin films, Materials 13 (2020) 518.
[27] A. Assy, S. Gomes, Temperature-dependent capillary forces at nano-contacts for estimating the heat conduction through a water meniscus, Nanotechnology 26 (2015), 355401.
[28] L. David, S. Gomes, M. Raynaud, Modeling for the thermal characterization of solid materials by DC scanning thermal microscopy, J. Phys. D Appl. Phys. 40 (2007) 4337–4346.
[29] J. Martinek, P. Klapetek, A. Charvátová Campbell, Methods for topography artifacts compensation in scanning thermal microscopy, Ultramicroscopy 155 (2015) 55–61.

[30] J. Wang, Z. Zhang, R. Shi, B.N. Chandrashekar, N. Shen, H. Song, N. Wang, J. Chen, C. Cheng, Impact of nanoscale roughness on heat transport across the solid–solid interface, Adv. Mater. Interfaces 7 (2020), 1901582.
[31] C.C. Leznoff, A.B.P. Lever, Phthalocyanines –Properties and Applications, Wiley-VCH, Weinheim, 1996.
[32] P.L. Ong, I.A. Levitsky, Organic/IV, III-V semiconductor hybrid solar cells, Energies 3 (2010) 313–334.
[33] S. Rajaputra, S. Vallurupalli, V.P. Singh, Copper phthalocyanine based schottky diode solar cells, J. Mater. Sci. Mater. Electron. 18 (2007) 1147–1150.
[34] P. Powroźnik, W. Jakubik, A. Kaźmierczak-Bałata, Detection of organophosphorus (DMMP) vapour using phthalocyanine-palladium bilayer structures, Procedia Eng. 120 (2015) 368–371.
[35] H. Aldahhak, P. Powroźnik, P. Pander, W. Jakubik, F.B. Dias, W.G. Schmidt, U. Gerstmann, M. Krzywiecki, Toward efficient toxic-gas detectors: exploring molecular interactions of sarin and dimethyl methylphosphonate with metal-centered phthalocyanine structures, J. Phys. Chem. C 124 (2020) 6090–6102, 11.
[36] http://gwyddion.net/ (accessed 29 November 2021).
[37] http://gwyddion.net/documentation/user-guide-en/statistical-analysis.html (accessed 29 November 2021).
[38] http://gwyddion.net/documentation/user-guide-en/grain-analysis.html (accessed 29 November).
[39] S. Lefèvre, 3ω-scanning thermal microscope, Rev. Sci. Instrum. 76 (2005), 033701.
[40] M. Chirtoc, J. Gibkes, R. Wernhardt, J. Pelzl, A. Wieck, Temperature-dependent quantitative 3ω scanning thermal microscopy: local thermal conductivity changes in NiTi microstructures induced by martensite-austenite phase transition, Rev. Sci. Instrum. 79 (2008), 093703.
[41] J. Bodzenta, J. Juszczyk, M. Chirtoc, Quantitative scanning thermal microscopy based on determination of thermal probe dynamic resistance, Rev. Sci. Instrum. 84 (2013), 093702.
[42] J. Juszczyk, A. Kaźmierczak-Bałata, P. Firek, J. Bodzenta, Measuring thermal conductivity of thin films by scanning thermal microscopy combined with thermal spreading resistance analysis, Ultramicroscopy 175 (2017) 81–86.
[43] E. Puyoo, S. Grauby, J.M. Rampnoux, E. Rouviere, S. Dilhaire, Thermal exchange radius measurement: application to nanowire thermal imaging, Rev. Sci. Instrum. 81 (2010), 073701.
[44] M. Pawlak, S. Pal, S. Scholz, A. Ludwig, A.D. Wieck, Simultaneous measurement of thermal conductivity and diffusivity of an undoped Al0.33Ga0.67As thin film epitaxially grown on a heavily Zn doped GaAs using spectrally-resolved modulated photothermal infrared radiometry, Thermochim. Acta 662 (2018) 69–74.
[45] M. Pawlak, N. Jukam, T. Kruck, D. Dziczek, A. Ludwig, A.D. Wieck, Measurement of thermal transport properties of selected superlattice and thin films using frequency-domain photothermal infrared radiometry, Measurement 166 (2020), 108226.
[46] D.S. Smith, A. Alzina, J. Bourret, B. Nait-Ali, F. Pennec, N. Tessier-Doyen, K. Odsu, H. Matsubara, P. Elser, U.T. Gonzenbach, Thermal conductivity of porous materials, J. Mater. Res. 28 (2013) 2260–2272.
[47] Y. Jin, A. Yadav, K. Sun, H. Sun, K.P. Pipe, M. Shtein, Thermal boundary resistance of copper phthalocyanine-metal interface, Appl. Phys. Lett. 98 (2011), 093305.
[48] Y. Jin, C. Shao, J. Kieffer, K.P. Pipe, M. Shtein, Origins of the boundary conductance of interfaces involving organic semiconductors, J. Appl. Phys. 112 (2012), 093503.
[49] S. Lefèvre, J.B. Saulnier, C. Fuentes, S. Volz, Probe Calibration of the scanning thermal microscope in the AC mode, Superlattice Microstruct. 35 (2004) 283–288.
[50] S. Lefèvre, S. Volz, P.O. Chapuis, Nanoscale heat transfer at contact between a hot tip and a substrate, Int. J. Heat Mass Trans. 49 (2006) 251–258.
[51] E. Guen, P.O. Chapuis, R. Rajkumar, P.S. Dobson, G. Mills, J.M.R. Weaver, S. Gomés, Scanning thermal microscopy on samples of varying effective thermal conductivities and identical flat surfaces, J. Appl. Phys. 128 (2020) 23530.
[52] E. Guen, Microscopie Thermique à Sonde Locale : étalonnages, Protocoles de Mesure et Applications Quantitatives Sur Des Matériaux Nanostructurés, INSA Lyon, 2020.
[53] M. Chirtoc, J. Bodzenta, A. Kaźmierczak-Bałata, Calibration of conductance channels and heat flux sharing in scanning thermal microscopy combining resistive thermal probes and pyroelectric sensors, Int. J. Heat Mass Trans. 156 (2020), 119860.